

Supplementary material for 'Intrinsically weak magnetic anisotropy of cerium in potential hard-magnetic intermetallics'

Anna Galler

*Centre de Physique Théorique, Ecole Polytechnique, CNRS,
Institut Polytechnique de Paris, 91128 Palaiseau Cedex, France*

Semih Ener, Fernando Maccari, Imants Dirba, Konstantin P. Skokov, and Oliver Gutfleisch

*Functional Materials, Department of Material Science,
Technische Universität Darmstadt, 64287, Darmstadt, Germany*

Silke Biermann

*Centre de Physique Théorique, Ecole Polytechnique, CNRS,
Institut Polytechnique de Paris, 91128 Palaiseau Cedex, France
Collège de France, 11 place Marcelin Berthelot, 75005 Paris, France
Department of Physics, Division of Mathematical Physics,
Lund University, Professorgatan 1, 22363 Lund, Sweden and
European Theoretical Spectroscopy Facility, 91128 Palaiseau, France, Europe*

Leonid V. Pourovskii

*Centre de Physique Théorique, Ecole Polytechnique, CNRS,
Institut Polytechnique de Paris, 91128 Palaiseau Cedex, France and
Collège de France, 11 place Marcelin Berthelot, 75005 Paris, France*

(Dated: December 17, 2020)

Supplementary Note 1: Details of the sample preparation and characterization

The polycrystalline samples used in this study were prepared by melting high-purity elements in an induction furnace under a purified argon atmosphere. The resulting ingots were suction-cast (arc melting/suction casting setup MAM-1 Edmund Bühler GmbH) from melt into bulk rectangular ingots of thickness 0.5mm to ensure fast solidification/cooling. To carry out the structural analysis, part of the sample was powdered and the resulting powder was used for room temperature x-ray diffraction (XRD). The XRD measurements were carried out on a Stoe Stadi P diffractometer with Mo $K\alpha_1$ radiation, in transmission mode and an angular 2θ range from 5° to 40° . Phase matching and unit-cell refinements were performed using FullProf software¹.

The remaining part of the sample was hand-grind in an agate mortar and sieved below $20\ \mu\text{m}$ in an Ar filled glovebox ($p(\text{O}_2)$ and $p(\text{H}_2\text{O}) < 0.1$ ppm, MBraun) for magnetic characterization and nitrogenation. Nitrogenation experiments were carried out in a custom-build horizontal quartz tube setup equipped with a furnace. The samples were transferred to the furnace without contact to air to avoid oxidation. A temperature of 670 K for 10 h in $100\ \text{cm}^3/\text{min}$ N_2 flow was used.

The room temperature XRD results indicate an almost phase-pure starting material with 96.6 ± 2.0 wt.% $\text{CeFe}_{11}\text{Ti}$ phase (with the unit cell parameters $a = 8.542 \pm 0.001\ \text{\AA}$ and $c = 4.788 \pm 0.001\ \text{\AA}$) obtained with a small fraction (3.36 ± 0.3 wt.%) of secondary CeFe_2 -Laves phase. After nitrogenation the unit cell parameters of the $\text{CeFe}_{11}\text{TiN}_x$ phase are measured as $a = 8.695 \pm 0.012\ \text{\AA}$ and $c = 4.902 \pm 0.012\ \text{\AA}$. The obtained unit cell parameters are in good agreement with results reported in the literature².

Isothermal magnetization measurements were performed on aligned powder samples using a PPMS-VSM (Quantum Design) under applied magnetic field up to 10 T. The powder consists of particles, assumed to be monocrystalline, with size less than $20\ \mu\text{m}$. The particles were mixed with paraffin wax and encapsulated in a metallic pan. Afterwards, the pan was heated above the melting point of the wax and an external magnetic field of 1.3 T was applied for texturing. Isothermal magnetization measurements were carried out in the temperature range of $5\text{K} \leq T \leq 300\text{K}$.

$M(T)_T$ curves measured perpendicular to the direction of the texture were used for the estimation of the anisotropy fields by using the method suggested by Durst and Kronmüller³. For cross-checking, room temperature anisotropy field estimations were done by using the classical Sucksmith-Thompson method⁴. Both methods coincide for the estimation of the anisotropy fields.

For the confirmation of the proper nitrogenation process thermomagnetic measurements were carried out and the Curie temperatures of $487 \pm 2\ \text{K}$ and $765 \pm 4\ \text{K}$ are obtained for $\text{CeFe}_{11}\text{Ti}$ and $\text{CeFe}_{11}\text{TiN}_x$, respectively, which agrees well with the previously reported literature.

Supplementary Note 2: Details of the DFT+DMFT calculations

In our DFT+DMFT calculations—carried out using the implementation in Refs. 5–8—we construct the projective Wannier functions to represent the subspace of the correlated Ce-4*f* states using the Kohn-Sham eigenstates enclosed by the energy window $[-1.36 : 2.72]$ eV around the Fermi level. The on-site screened Coulomb interaction within the Ce-4*f* subspace was defined by $F^0 = U = 6$ eV, $J_H = 0.7$ eV, these values are in agreement with cRPA calculations^{9,10} as well as the usual range for these parameters for Ce intermetallics^{11–13}.

In the Ce-4*f* quantum impurity problem we treat all fourteen Ce-4*f* orbitals as correlated and employ the density-density approximation for the corresponding Coulomb vertex. We verified that for the particular case of the Ce- f^1 shell the density-density approximation is reliable for calculations of the Kondo scale, which is expected to be very sensitive to the treatment of the ground-state splitting. First, since the quasi-atomic ground-state occupancy of Ce-4*f* is $n_{at} = 1$, the splitting of the ground-state $N = 1$ levels is not affected by the Coulomb interaction. Another important factor is the energy splitting between the ground state and excited states with occupancies $N - 1$ and $N + 1$. With the hybridization effects included in QMC the most important valence fluctuations for Ce are $f^1 \rightarrow f^0$, resulting in a reduction of the occupancy below 1 ($n_f = 0.94$ and $n_f = 0.84$ in CeFe₁₁Ti and CeFe₁₁TiN, respectively). The energy cost of those fluctuations is not affected by Hund’s rule coupling. Moreover, as we verified by comparing the quasiatomic spectra for Ce-4*f* calculated with the full and density-density vertices, the splitting between the top of the lower Hubbard band and the bottom of the higher one is very well reproduced by the density-density approximation. Hence, the $f^1 \rightarrow f^2$ valence fluctuations, which are less important in Ce than $f^1 \rightarrow f^0$, are anyway quite well accounted for within the density-density approximation.

The employed double-counting scheme is the fully localized double counting, i.e. the formula $E_{DC} = U(n_{at} - 0.5) - J(0.5n_{at} - 0.5)$ with the atomic occupancy ($n_{at} = 1$ for Ce³⁺), which has been shown appropriate for the self-consistent DFT+HubI method¹⁴. A stochastic maximum-entropy algorithm¹⁵ is used for the analytical continuation of the converged DMFT(QMC) Matsubara self-energy to the real axis.

The intermetallic phases CeFe₁₁Ti and CeFe₁₁TiN crystallize in a tetragonal body-centered lattice structure, space group $I4/mmm$. The conventional unit cell (shown in the inset of Fig. 1 in the main text), containing two formula units, is orthorhombic. It has equivalent Ce sites in the corner and the center at Wyckoff position $2a$, N interstitial sites between two nearest Ce sites at Wyckoff position $2b$, and three inequivalent Fe sites at Wyckoff positions $8i$, $8j$ and $8f$, respectively.

The results presented in the main text were calculated using theoretical lattice structures of the Ce-Fe ”1-12” systems that were obtained as described in the following.

The inner coordinate x of the Fe sites $8i$ and $8j$, which have never, to our awareness, been measured experimentally in Ce ”1-12” intermetallics, were fixed in our calculations to 0.359 and 0.27, respectively, in accordance with the results of Ref. 16 on the Nd ”1-12” system. In CeFe₁₁Ti(N), Ti occupies one of the Fe($8i$) sites, for which we assumed the same internal parameter as for Fe($8i$). We obtained the lattice parameters of parent CeFe₁₂, which cannot be stabilized experimentally, by a volume optimization within DFT+U. The resulting values $a=8.40$ Å, $c=4.81$ Å were also used in the calculations of CeFe₁₁Ti. For CeFe₁₁TiN we employed the theoretical lattice parameters $a=8.51$ Å, $c=4.88$ Å. They were evaluated assuming a uniform volume expansion of about 4% through nitrogenation with respect to CeFe₁₁Ti; this volume expansion is consistent with the experimental one of 6% in CeFe₁₁TiN _{x} (Supplementary Note 1) with x in the range from 1.5 to 2, a somewhat smaller expansion of 3.4% was reported by Ref.¹⁷ for $x=1.5$. We notice that the precise lattice parameters of CeFe₁₁TiN have not been so far established experimentally due to uncertainty in the nitrogen content.

To verify the sensitivity of our conclusions upon the change of the lattice parameters we also performed calculations for CeFe₁₁Ti using the experimental lattice constants reported in Supplementary Note 1, above. In this case we have also performed an optimization of the internal coordinates by minimizing the forces within DFT-GGA (neither fully localized nor fully itinerant treatment of Ce-4*f* is expected to be fully quantitatively adequate in the case of CeFe₁₁Ti). The Ce-Ti distance was found to increase by 5% compared to the one in the unrelaxed structure, while the opposite Ce-Fe($8i$) bond, in contrast, contracted by about 4%; other changes in internal coordinates due to structural relaxation were found to be small. Using the thus obtained optimized structure at the experimental lattice parameters we performed the same calculations of the Ce-4*f* magnetization and magnetic anisotropy. The obtained zero-temperature quasi-atomic Ce-4*f* magnetic moment is $M_z^{at}=0.95 \mu_B$; the DMFT(QMC) Ce-4*f* moment $M_z=0.25 \mu_B$ is nearly constant at low T . The resulting reduction of this moment by Kondo screening, $\alpha^2 = M_z(T=0)/M_z^{at}(T=0) = 0.26$ is very similar to that obtained with the theoretical lattice structure and reported in Fig. 2a of the main text. We subsequently estimated the K_1 anisotropy constant of screened Ce-4*f* using Eq. (4) of the main text and adopting the same value of $A = 770$ K as for the theoretical structure. The resulting CeFe₁₁Ti anisotropy field of 5.3 T at $T = 4.2$ K is again similar to that obtained with the theoretical structure (cf. Table II of the main text).

We also calculated CeFe₁₁TiN assuming the experimental lattice parameters of CeFe₁₁TiN _{x} reported in the Supplementary Sec. I and using the same approach, i. e. charge self-consistent DFT+HubI followed by DMFT(QMC). The

resulting low- T moment on Ce of about $0.06 \mu_B$ indicates a robustly strong Kondo screening and, correspondingly, a robust suppression of the Ce-4 f single-ion anisotropy in CeFe₁₁TiN.

Supplementary Note 3: Zero-temperature anisotropy of the Kondo-screened moment under an applied exchange field

We consider the following multiband Kondo-like (Coqblin-Schriffer) model for a local moment with the total angular momentum J^f coupled to conduction-electron bands:

$$H = H_c + H_K + H_B + H_{CF} = \sum_{\mathbf{k}\mu b} \epsilon_{\mathbf{k}b\mu} c_{\mathbf{k}\mu b}^\dagger c_{\mathbf{k}\mu b} + \sum_{\substack{\mu\mu' \\ \mathbf{k}\mathbf{k}'b b'}} J_{\mu\mu'}^{\mathbf{k}b\mathbf{k}'b'} \hat{X}_{\mu'\mu} c_{\mathbf{k}\mu b}^\dagger c_{\mathbf{k}'\mu'b'} + \sum_a B_{ex}^a \hat{S}_a^f + B_2^0 \hat{C}_2^0, \quad (1)$$

where $c_{\mathbf{k}\mu b}^\dagger$ ($c_{\mathbf{k}\mu b}$) creates (annihilates) the conduction-electron state with the angular momentum μ at the Brillouin zone point \mathbf{k} and band b , H_K is the antiferromagnetic coupling of the local impurity and conduction-electron, which we write in a general form using the \mathbf{k} , band and μ -dependent Kondo coupling $J_{\mu\mu'}^{\mathbf{k}b\mathbf{k}'b'}$ between conduction electrons and the Hubbard operators $\hat{X}_{\mu'\mu} \equiv |\mu'\rangle\langle\mu|$. The exchange field B_{ex}^a , $a = x, y, z$, acts on the corresponding projection of the local spin \hat{S}_a^f . The last term is the crystal field (CF), which we define for simplicity as the lowest-rank term of the tetragonal CF inducing the anisotropy of the local moment, where $B_2^0 = 2\alpha_J A_2^0 \langle r^2 \rangle$ is the CF parameter for the angular momentum quantum number $l=2$ and its projection $m=0$; \hat{C}_2^0 is the corresponding spherical tensor in the Stevens normalization, $\alpha_J = -2/35$ is the Stevens factor for $J = 5/2$. Restricting the consideration to the Ce-4 f ground-state multiplet $J^f = 5/2$ one may rewrite the tensor in the operator-equivalent form $\hat{C}_2^0 = \frac{3}{2} \left([\hat{J}_z^f]^2 - J^f(J^f + 1)/3 \right) = \frac{3}{2} [\hat{J}_z^f]^2 - 35/8$.

We assume the ground state (GS) of the Hamiltonian (1) to be given by the following variational many-electron wave function:

$$\Psi = \sqrt{1 - \alpha^2} \Psi_S + \alpha \Psi_J, \quad (2)$$

Ψ_S in the first term is a singlet state of the local moment and conduction electron:

$$\Psi_S = \sum_{\mu} \gamma_{\mu} (|J^f, \mu\rangle |c_{\bar{\mu}}\rangle - |J^f, -\mu\rangle |c_{\mu}\rangle), \quad (3)$$

where $\bar{\mu} = -\mu$, $|c_{\mu}\rangle$ is a state of the perturbed Fermi sea with a conduction electron angular momentum excitation μ , $|J^f, \mu\rangle$ is the eigenstate of \hat{J}_z^f of local moment with the angular-momentum projection μ , $\hat{J}_z^f |J^f, \mu\rangle = \mu |J^f, \mu\rangle$. The unperturbed Fermi sea reads $\Psi_{FS} = \sum_{\substack{\mathbf{k}\mu b \\ \epsilon_{\mathbf{k}b\mu} < E_F}} c_{\mathbf{k}\mu b}^\dagger c_{\mathbf{k}\mu b} |0\rangle$; it is the ground state of the first term H_c in (1).

The second contribution into Ψ reads

$$\Psi_J = \left[\sum_{\mu} \beta_{\mu} |J^f, \mu\rangle \right] \Psi_{FS}, \quad (4)$$

where the prefactors β_{μ} are chosen so that Ψ_J is the normalized GS of the terms $H_c + H_B + H_{CF}$ in the Hamiltonian (1). In the present case of a Kramers ion Ce³⁺ in a strong exchange field B_{ex} this GS is expected to be non-degenerate.

Finally, α is the variational parameter chosen to minimize the total energy of Ψ ,

$$\frac{\partial \langle \Psi | H | \Psi \rangle}{\partial \alpha} = 0. \quad (5)$$

Several comments are in order regarding the variational wavefunction Ψ :

- the singlet part Ψ_S is written in a general variational form, similarly to various *ansatz* for the Kondo-problem ground state used previously for Kondo and generalized Anderson impurity Hamiltonians¹⁸⁻²⁰ and consists of a superposition of the angular momentum projections $\mu(\bar{\mu})$ coupled to a conduction-electron excitation $|c_{\bar{\mu}}\rangle$ ($|c_{\mu}\rangle$) of the opposite momentum direction, thus forming a singlet. Notice that the states $|c_{\bar{\mu}}\rangle$ are not restricted to

single conduction-electron excitations of Ψ_{FS} . These states can comprise an arbitrary number of elementary of those excitations, e. g.:

$$|c_{\bar{\mu}}\rangle = \sum_{\substack{bb_1b_2b_3\dots \\ \mathbf{k}\mathbf{k}_1\mathbf{k}_2\mathbf{k}\dots \\ \mu\bar{\mu}\mu_1\dots}} \gamma(b, b_1, b_2, \dots, \mathbf{k}, \mathbf{k}_1, \mathbf{k}_2, \dots, \mu, \bar{\mu}, \mu_1, \dots) c_{\mathbf{k}\bar{\mu}b}^\dagger c_{\mathbf{k}_1\mu b_1} c_{\mathbf{k}_2\mu_1 b_2}^\dagger c_{\mathbf{k}_3\mu_1 b_3} \dots \Psi_{FS}, \quad (6)$$

where the amplitudes γ can be treated as variational parameters. In result of its complicated structure with a lot of variational freedom, Ψ_S can be expected to provide a good estimated for the true ground state of quantum impurity in the absence of exchange field (for the Hamiltonian $H_c + H_K$) as obtained by exact techniques like the QMC. The precise form of Ψ_S is not important for the present derivation, which is based only on some its orthogonality properties specified below. We, however, assume Ψ_S to be rotationally invariant, which is a reasonable approximation in the present case of $T_K > \Delta_{CF}$, where Δ_{CF} is the total CF splitting. Indeed, as shown in Supplementary Fig. 3, the low-energy behavior of the QMC self-energy is almost the same for all six $j = 5/2$ orbitals implying very similar renormalization due to the Kondo interaction.

- The second term, Ψ_J , is the solution of Hamiltonian (1) in the absence of Kondo coupling. Hence, the variational wavefunction (2) is the superposition of solutions in two limits $H_K = 0$ and $H_B = 0$.
- The unperturbed Fermi sea Ψ_{FS} in (2) can be spin-polarized. A spin-polarized conduction sea does not prevent the Kondo effect to occur as far as this spin polarization is not complete; hence, the conduction-electron bands of both spins contribute to the Fermi surface. That spin polarization is not important for the derivation, since the only property we use is Ψ_{FS} being the same in the both terms of (2).

From the general form of the variational wavefunction Ψ one may easily derive the following properties:

- $\langle \Psi_S | \hat{J}_a^f | \Psi_S \rangle = 0$ for $a = x, y, z$, hence,

$$\langle \Psi | \hat{J}_a^f | \Psi \rangle = \alpha^2 \langle \Psi_J | \hat{J}_a^f | \Psi_J \rangle \text{ and} \quad (7)$$

$$\langle \Psi_S | H_B | \Psi_S \rangle = 0, \quad (8)$$

which follows from the singlet form of Ψ_S and the orthogonality between the Fermi-sea excitations, $\langle c_{\bar{\mu}} | c_{\mu} \rangle = 0$. Moreover, under the rotationally-invariant approximation for Ψ_S discussed above one also has

$$\langle \Psi_S | H_{CF} | \Psi_S \rangle = 0. \quad (9)$$

- The terms H_B and H_{CF} do not couple Ψ_S and Ψ_J :

$$\langle \Psi_S | H_B | \Psi_J \rangle = 0, \quad (10)$$

$$\langle \Psi_S | H_{CF} | \Psi_J \rangle = 0, \quad (11)$$

as follows from the orthogonality properties $\langle c_{\bar{\mu}} | c_{\mu} \rangle = 0$, $\langle c_{\mu} | \Psi_{FS} \rangle = 0$ and $\langle c_{\bar{\mu}} | \Psi_{FS} \rangle = 0$.

When $\vec{B}_{ex} || z$ the exchange-field term becomes $H_B = B_{ex} \hat{S}_z^f = \Delta_{ex} \hat{J}_z^f$, where $\Delta_{ex} = 2(g_J - 1)B_{ex} = -2B_{ex}/7$, with the value $g_J = 6/7$ for the gyromagnetic ratio for the $J = 5/2$ multiplet substituted into the RHS. The contribution of the last two terms in (1) to the GS energy then reads

$$\langle \Psi | H_B + H_{CF} | \Psi \rangle = \alpha^2 \langle J^f, J^f | H_B + H_{CF} | J^f, J^f \rangle = \alpha^2 [\Delta_{ex} J^f + B_2^0 J^f (J^f - 1/2)], \quad (12)$$

where the properties (7)-(11) were used in the first line. In the second one we used the fact that the wavefunction $|J^f, J^f\rangle$ is the $4f$ ground state of $H_B + H_{CF}$ in the case of $\Delta_{ex} < 0$ and $B_2^0 < 0$ (as in CeFe₁₁Ti and CeFe₁₁TiN).

Let us now consider the change of energy $\Delta E(\alpha)$ upon the rotation of B_{ex} . We specify the direction of the exchange field $B_{ex}(\theta)$ by its angle θ with respect to the z axis (parallel to the c lattice parameter of the tetragonal unit cell) and confine this rotation to the xz plane. We thus neglect the polar-angle dependence of the magnetic anisotropy, which is insignificant in the CeFe₁₁ MX materials' family.

First we consider ΔE at the value of $\alpha = \alpha_0$, where α_0 was fixed by the minimization, Eq. 5, at $\theta = 0$, giving the variational ground-state energy E_{α_0} and wave function Ψ_0 . Then we evaluate

$$\Delta E(\alpha_0, \theta) = \text{MIN} [\langle \Psi | H(\theta) | \Psi \rangle]_{\alpha_0} - E_{\alpha_0},$$

where the minimization is assumed to be over all variational parameters in Ψ , i. e., β_μ , $\gamma_\mu, \gamma(b, b_1, b_2, \dots, \mathbf{k}, \mathbf{k}_1, \mathbf{k}_2, \dots, \mu, \bar{\mu}, \mu_1, \dots)$, see eqs. 3, 4 and 6, apart from α fixed at α_0 .

In order to evaluate $\text{MIN}[\langle \Psi | H(\theta) | \Psi \rangle]_{\alpha_0}$ one may employ, e.g., first order perturbation theory with respect to H_{CF} that is treated as a smaller term compared to H_B . Namely, we rotate the local coordinate frame by the angle θ so that the resulting axis $\hat{z} || B_{ex}(\theta)$, hence, the form of H_B in the new frame is the same, $\Delta_{ex} \hat{J}_z^f$. Correspondingly, Ψ_J takes the same form $|J^f, J^f\rangle$ in the new frame, and Ψ_S is rotationally invariant. The perturbation term in H_{CF} due to the substitution $\hat{J}_z \rightarrow \hat{J}_z \cos \theta - \hat{J}_x \sin \theta$ reads

$$\Delta H_{CF}(\theta) = -\frac{3B_2^0}{2} [\hat{J}_z^2 \sin^2 \theta - \hat{J}_x^2 \sin^2 \theta + (\hat{J}_z \hat{J}_x + \hat{J}_x \hat{J}_z) \sin 2\theta]. \quad (13)$$

Using (9) and (11) one thus obtains

$$\text{MIN}[\langle \Psi | H(\theta) | \Psi \rangle]_{\alpha_0} - E_{\alpha_0} = \langle \Psi_0 | \Delta H_{CF}(\theta) | \Psi_0 \rangle = \alpha_0^2 \langle J^f, J | \Delta H_{CF}(\theta) | J^f, J \rangle$$

with only the first two terms in (13) contributing to the first-order correction $\langle J^f, J | \Delta H_{CF}(\theta) | J^f, J \rangle$. A straightforward calculation gives

$$\langle J^f, J^f | \Delta H_{CF}(\theta) | J^f, J^f \rangle = -3/2 B_2^0 J^f (J^f - 1/2) \sin^2 \theta \equiv K_1^{at} \sin^2 \theta, \quad (14)$$

where

$$K_1^{at} = -3/2 B_2^0 J^f (J^f - 1/2) = -3\alpha_J^f A_2^0 \langle r^2 \rangle J^f (J^f - 1/2) \quad (15)$$

coincides, as expected, with the standard expression for the exchange-dominated limit at zero temperature²¹. Therefore, for the full K_1 anisotropy constant of the screened local moment (1) we obtain

$$K_1(\alpha_0) = \alpha_0^2 K_1^{at}. \quad (16)$$

At the same time, according to Eq. 7, α_0 scales also the local moment

$$\langle \hat{J}_z \rangle = \langle \Psi | \hat{J}_z^f | \Psi \rangle = \alpha_0^2 \langle \Psi_J | \hat{J}_z^f | \Psi_J \rangle = \alpha_0^2 \langle \hat{J}_z^{at} \rangle. \quad (17)$$

Thus, we extract the value of α_0 from the ratio of Ce moments calculated at $\vec{B}_{ex} || c$ with the full solution in DMFT(QMC) and within the atomic approximation (DFT+HubI). Explicitly,

$$\alpha_0^2 = \frac{\langle \hat{J}_z \rangle}{\langle \hat{J}_z^{at} \rangle} = \frac{\langle \hat{M}_z \rangle}{\langle \hat{M}_z^{at} \rangle}, \quad (18)$$

where the ratio $\frac{\langle M_z \rangle}{\langle M_z^{at} \rangle}$ can be extracted by extrapolating the curves $M_z(T)$ (Fig. 2a of the main text) to zero temperature.

Let us now consider the effect of θ -dependence of the variational parameter α on the anisotropy constant. We thus assume the expectation value of the Hamiltonian (1) for the variational wave function (2) to be in the following form:

$$E(\alpha, \theta) = A(\alpha - \alpha_0)^2 + K_1^{at} \alpha^2 \sin^2 \theta + O(\alpha^{n \geq 4}), \quad (19)$$

where the first term is due to the condition (5) at $B_{ex}(\theta = 0)$, the second one is the anisotropy energy (21) at a given value of α . As we are primarily interested in describing the anisotropy for large θ (easy vs. hard direction) we fix $\theta = \pi/2$ and minimize $E(\alpha, \pi/2)$ with respect to α obtaining $\alpha = \frac{A\alpha_0}{A + K_1^{at}}$. Inserting this into (19) we find the energy correction to be

$$E(\alpha, \pi/2) - E(\alpha_0, \pi/2) = -\alpha_0^2 K_1^{at} \frac{\delta}{1 + \delta}, \quad (20)$$

with $\delta = K_1^{at}/A$. Thus, the final formula for the anisotropy constant that we use reads

$$K_1 = \alpha_0^2 K_1^{at} \left(1 - \frac{\delta}{1 + \delta} \right) = \alpha_0^2 K_1^{at} \frac{1}{1 + \delta} \quad (21)$$

where K_1^{at} is given by Eq. 15 and α_0^2 by Eq. 7.

The parameter A , giving the curvature of $E(\alpha, \theta = 0)$ in Eq. 19), we evaluate by explicitly varying the magnitude of the exchange field B_{ex} while keeping its direction aligned to c ; this calculation can easily be done within our DMFT(QMC) framework. Then, by minimizing the corresponding expression for the variational total energy

$$E(\alpha) = A(\alpha - \alpha_0)^2 - B_{ex}\hat{S}_z^f = A(\alpha - \alpha_0)^2 - \Delta_{ex}\alpha^2 \quad (22)$$

with respect to α , we finally obtain

$$A = -\frac{\Delta_{ex}\alpha}{\alpha - \alpha_0}, \quad (23)$$

where α_0 corresponds to the ratio of moments in Eq. 18 with $B_{ex}||c$, whereas α represents the same ratio with increased exchange field, i.e. additional Δ_{ex} applied. The corresponding values for A are 770, 475 K for CeFe₁₁Ti and CeFe₁₁TiN, respectively.

Supplementary Note 4: Crystal-field parameters and anisotropy constants in CeFe₁₁M(N)

The quasi-atomic Hamiltonian for the Ce-4*f* shell reads:

$$\hat{H}_{at} = \hat{H}_{1el} + \hat{H}_U = \sum_{mm'\sigma\sigma'} \epsilon_{mm'\sigma\sigma'}^\dagger f_{m\sigma}^\dagger f_{m'\sigma'} + \hat{H}_U, \quad (24)$$

where \hat{H}_U is the on-site Coulomb repulsion, and the one-electron 4*f* level positions read

$$\hat{\epsilon} = \hat{E}_0 + \lambda \sum_i s_i l_i + \hat{H}_{cf} + \hat{H}_{ex} \quad (25)$$

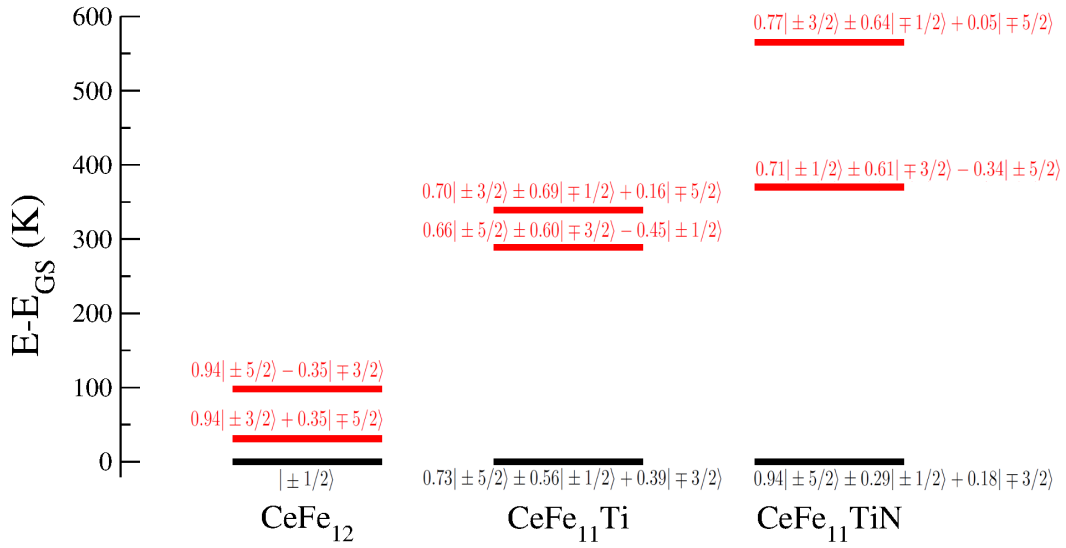
where the terms on the right hand side are the uniform shift as well as the spin-orbit, crystal field (CF), and exchange field. The exchange field is $\hat{H}_{ex} = 2\mu_B B_{ex} \mathbf{n} \hat{\mathbf{S}}_f$, where the exchange field B_{ex} along the direction \mathbf{n} is due to the magnetic transition-metal sublattice coupled to the Ce-4*f* spin $\hat{\mathbf{S}}_f$. The CF Hamiltonian is defined by crystal field parameters (CFPs) in the standard $A_l^m \langle r^l \rangle$ notation, in the case of a tetragonal point-group symmetry only the CFPs for the following lm combinations can be non-zero: 20, 40, 44, 60, and 64. Although in the case of CeFe₁₁Ti and CeFe₁₁TiN the point group of the Ce site is orthorhombic, the effect of the corresponding non-tetragonal CFPs is cancelled by a random distribution of Ti substitutions restoring the original tetragonal symmetry.

In Supplementary Table I we list the CFPs and exchange field in the three intermetallics calculated by DFT+HubI. One sees that the low-rank "20" parameter is largest in CeFe₁₁TiN; in all three compounds the high-rank CFPs are large thus substantially affecting the anisotropy at low temperatures.

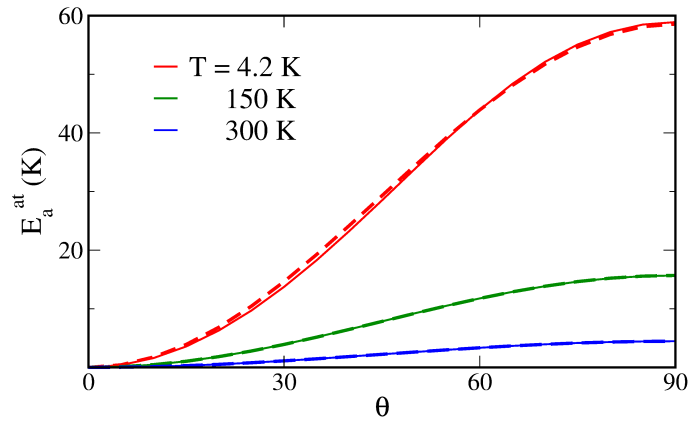
In order to evaluate the anisotropy constants we employ a numerical diagonalization of the Hamiltonian (24) to calculate its free energy $F(\mathbf{n})$ as a function of the direction of the exchange field \mathbf{n} . We parametrize \mathbf{n} by the angle θ with respect to the tetragonal c axis in the ac plane. The resulting dependence of the Ce single-ion anisotropy energy $E_a^{at} = F(\theta) - F(\theta = 0)$ for CeFe₁₁Ti is shown in Supplementary Fig. 2 for several temperatures. One sees that the resulting dependence is very well described by only one anisotropy constant $E_a^{at} \approx K_1^{at} \sin^2 \theta$. For CeFe₁₁TiN the fit with only K_1^{at} is worse, however, we keep this basic fit in view of simplifying the subsequent treatment of the Kondo screening, which will, as shown in the main text, almost completely suppress the Ce single-ion contribution in the case of CeFe₁₁TiN.

Supplementary Table I: Calculated crystal-field parameters (in K) and exchange field (in Tesla)

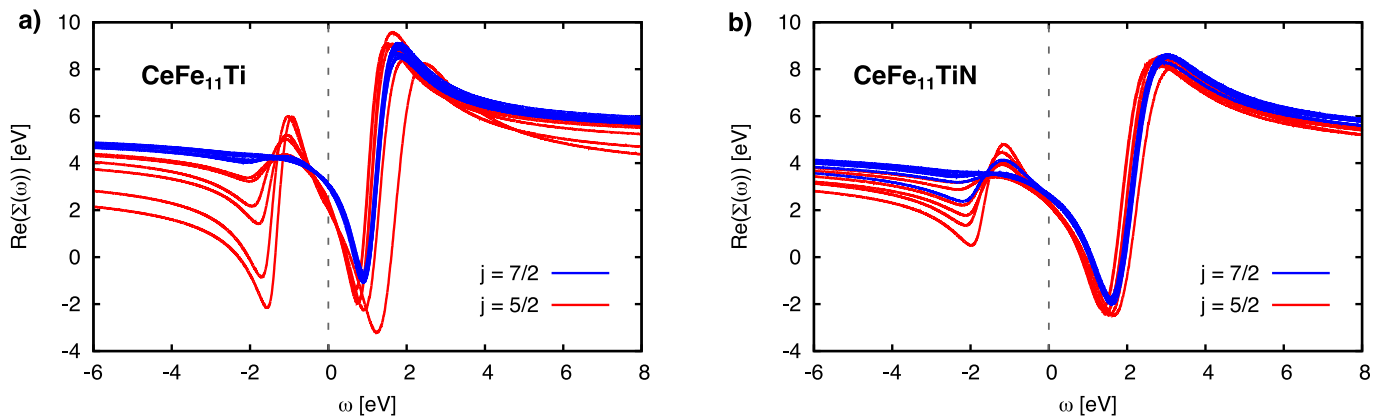
| | $A_2^0 \langle r^2 \rangle$ | $A_4^0 \langle r^4 \rangle$ | $A_4^4 \langle r^4 \rangle$ | $A_6^0 \langle r^6 \rangle$ | $A_6^4 \langle r^6 \rangle$ | B_{ex} |
|------------------------|-----------------------------|-----------------------------|-----------------------------|-----------------------------|-----------------------------|----------|
| CeFe ₁₂ | -58 | 0 | -123 | 105 | 94 | 306 |
| CeFe ₁₁ Ti | 137 | -34 | -424 | 130 | 177 | 320 |
| CeFe ₁₁ TiN | 424 | -91 | -358 | -86 | 242 | 220 |



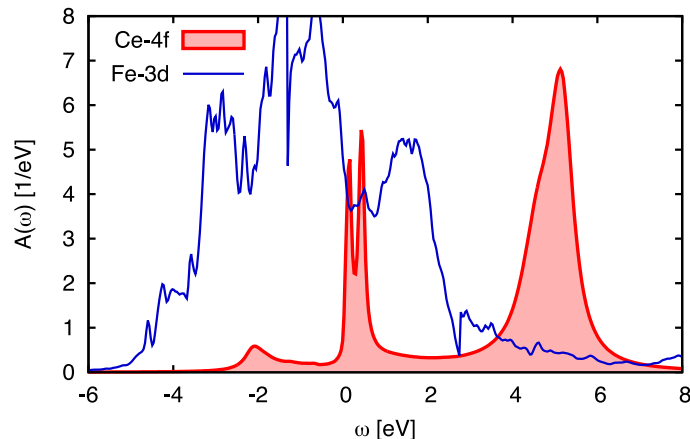
Supplementary Figure 1: Crystal-field splitting and eigenstates in $\text{CeFe}_{11}M(N)$ intermetallics. The figure shows the crystal field splitting of the $J = 5/2$ multiplet and the resulting eigenstates obtained for CeFe_{12} , $\text{CeFe}_{11}\text{Ti}$ and $\text{CeFe}_{11}\text{TiN}$ using the DFT+HubI approach.



Supplementary Figure 2: Anisotropy energy in $\text{CeFe}_{11}\text{Ti}$ calculated by numerical diagonalization of the Hamiltonian (24) (solid lines) compared to its fit to the form $\approx K_1^{at} \sin^2 \theta$ (dashed lines).



Supplementary Figure 3: Orbital-resolved DMFT(QMC) self-energies. **(a)** In $\text{CeFe}_{11}\text{Ti}$, the main visible difference at low energies is between the orbitals belonging to the excited atomic multiplet $J = 7/2$ (in blue) and the $J = 5/2$ orbitals belonging to the atomic ground state multiplet (in red). Note that the $J = 7/2$ orbitals are almost empty, while the $J = 5/2$ orbitals carry $n_{5/2} = 0.82$ of a total Ce-4f filling of $n_f = 0.94$. **(b)** In $\text{CeFe}_{11}\text{TiN}$, the difference between the $J = 5/2$ and the $J = 7/2$ manifold is still clearly visible, but the occupancy of the $J = 7/2$ orbitals has increased. The $J = 5/2$ orbitals carry now $n_{5/2} = 0.60$ of a total $n_f = 0.84$.



Supplementary Figure 4: DMFT(QMC) spectral function of CeFe_{12} . The Fe spectral weight has been rescaled by a factor $1/3$. The Ce-4f occupancy is $n_f = 0.93$.

-
- ¹ J. Rodríguez-Carvajal, *Physica B: Condensed Matter* **192**, 55 (1993).
 - ² C. Zhou, F. Pinkerton, and J. Herbst, *Cerium-iron-based magnetic compounds* (2013), US Patent 9,548,150 B2.
 - ³ K.-D. Durst and H. Kronmüller, *Journal of Magnetism and Magnetic Materials* **59**, 86 (1986).
 - ⁴ W. Sucksmith and J. E. Thompson, *Proc. R. Soc. Lond. A.* **225**, 365 (1954).
 - ⁵ M. Aichhorn, L. Pourovskii, V. Vildosola, M. Ferrero, O. Parcollet, T. Miyake, A. Georges, and S. Biermann, *Phys. Rev. B* **80**, 085101 (2009).
 - ⁶ M. Aichhorn, L. Pourovskii, and A. Georges, *Phys. Rev. B* **84**, 054529 (2011).
 - ⁷ O. Parcollet, M. Ferrero, T. Ayrat, H. Hafermann, I. Krivenko, L. Messio, and P. Seth, *Computer Physics Communications* **196**, 398 (2015).
 - ⁸ M. Aichhorn, L. Pourovskii, P. Seth, V. Vildosola, M. Zingl, O. E. Peil, X. Deng, J. Mravlje, G. J. Kraberger, C. Martins, et al., *Computer Physics Communications* **204**, 200 (2016).
 - ⁹ S. Panda and S. Biermann (in preparation).
 - ¹⁰ F. Aryasetiawan, M. Imada, A. Georges, G. Kotliar, S. Biermann, and A. I. Lichtenstein, *Phys. Rev. B* **70**, 195104 (2004).
 - ¹¹ L. V. Pourovskii, P. Hansmann, M. Ferrero, and A. Georges, *Phys. Rev. Lett.* **112**, 106407 (2014).
 - ¹² K. Haule, C.-H. Yee, and K. Kim, *Phys. Rev. B* **81**, 195107 (2010).
 - ¹³ E. A. Goremychkin, H. Park, R. Osborn, S. Rosenkranz, J.-P. Castellan, V. R. Fanelli, A. D. Christianson, M. B. Stone,

- E. D. Bauer, K. J. McClellan, et al., *Science* **359**, 186 (2018).
- ¹⁴ L. V. Pourovskii, B. Amadon, S. Biermann, and A. Georges, *Phys. Rev. B* **76**, 235101 (2007).
- ¹⁵ K. S. D. Beach, *cond-mat/0403055*.
- ¹⁶ Y. Harashima, K. Terakura, H. Kino, S. Ishibashi, and T. Miyake, *Journal of Applied Physics* **120**, 203904 (2016).
- ¹⁷ M. Akayama, H. Fujii, K. Yamamoto, and K. Tatami, *Journal of Magnetism and Magnetic Materials* **130**, 99 (1994), ISSN 0304-8853.
- ¹⁸ K. Yosida and A. Yoshimori, in *Magnetism, Vol. V*, edited by R. G. T. and H. Suhl (New York: Academic Press, 1973), pp. 149 – 233.
- ¹⁹ C. M. Varma and Y. Yafet, *Phys. Rev. B* **13**, 2950 (1976).
- ²⁰ O. Gunnarsson and K. Schönhammer, *Phys. Rev. B* **28**, 4315 (1983).
- ²¹ M. Kuz'min and A. Tishin, in *Handbook of Magnetic Materials, Vol. 17*, edited by K. Buschow (Elsevier, 2007), pp. 149 – 233.